Received: 24 March 2020 | Revised: 2 July 2020 | Accepted: 13 July 2020 | Published online: 13 October 2020

DOI: 10.1002/dad2.12088

Alzheimer's & Dementia
Diagnosis, Assessment & Disease Monitoring

RESEARCH ARTICLE

Detection of presymptomatic Alzheimer's disease through breath biomarkers

Shadi Emam[1] | **Mehdi Nasrollahpour**[1] | **Bradley Colarusso**[2] | **Xuezhu Cai**[2] | **Simone Grant**[3] | **Praveen Kulkarni**[2] | **Adam Ekenseair**[3] | **Codi4 Gharagouzloo**[4] | **Craig F. Ferris**[2] | **Nian-Xiang Sun**[1]

[1] Department of Electrical and Computer Engineering, Advanced Materials and Microsystems Laboratory, Northeastern University, Boston, Massachusetts, USA

[2] Department of Psychology, Center for Translational NeuroImaging, Northeastern University, Boston, Massachusetts, USA

[3] Department of Chemical Engineering, Northeastern University, Boston, Massachusetts, USA

[4] Imaginostics, Inc., Northeastern University, Cambridge, Massachusetts, USA

Correspondence
Nian-Xiang Sun, Department of Electrical and Computer Engineering, Northeastern University, 417 Dana Research Center, 360 Huntington Ave, Boston, MA 02115-5000, USA.
Email: nian@ece.neu.edu

Abstract

Introduction: Novel sensors were developed to detect exhaled volatile organic compounds to aid in the diagnosis of mild cognitive impairment associated with early stage Alzheimer's disease (AD). The sensors were sensitive to a rat model that combined the human apolipoprotein E (APOE)4 gene with aging and the Western diet.

Methods: Gas sensors fabricated from molecularly imprinted polymer-graphene were engineered to react with alkanes and small fatty acids associated with lipid peroxidation. With a detection sensitivity in parts per trillion the sensors were tested against the breath of wild-type and APOE4 male rats. Resting state BOLD functional connectivity was used to assess hippocampal function.

Results: Only APOE4 rats, and not wild-type controls, tested positive to several small hydrocarbons and presented with reduced functional coupling in hippocampal circuitry.

Discussion: These results are proof-of-concept toward the development of sensors that can be used as breath detectors in the diagnosis, prognosis, and treatment of presymptomatic AD.

KEYWORDS
2,3-dimethylheptane, APOE4, butylated hydroxytoluene, electrochemical polymerization, hippocampal circuitry, imprinted polymer-graphene, lipid peroxidation, pivalic acid, resting state functional connectivity, silicon substrate, Western diet

1 | INTRODUCTION

Alzheimer's disease (AD) is a progressive degenerative brain disorder and the major cause of dementia in the world today.[1] In the United States alone, more than 5 million people have AD, a number expected to exceed 14 million by 2060.[2] AD is a contributing factor and a major cause of death in the U.S. population that is 65 years of age or older.[3] The cost for health care is staggering and projected to be >$500 billion annually in the United States by the year 2040.[4] The pathophysiology contributing to AD typically begins decades before any signs of cognitive dysfunction.[5] Amyloid beta (Aβ) plaques and neurofibrillary tangles are the pathological hallmarks of late stage AD.[6] Early diagnosis for risk of AD during the prodromal phase has driven the development of molecular biomarkers, many of which have focused on the chemistry of Aβ.[7]

Efforts to treat AD have also focused on molecular processes contributing to the Aβ cascade hypothesis. This longstanding hypothesis promotes the idea that AD is caused by plaques formed by the

aggregation and deposition of Aβ protein in brain parenchyma and the cascade of neuropathology that follows including tau hyperphosphorylation and formation of neurofibrillary tangles (NFTs), neuroinflammation, small vessel disease, neuronal death, and dementia.[8] A battery of biomarkers was developed for this cascade to assess key molecules in blood and cerebrospinal fluid together with cognitive and neuroimaging measures to follow disease progression and efficacy of new therapeutics.[9] Indeed, amyloid biomarkers are entry criterion in most late phase disease modifying clinical trials.[10] Unfortunately, the Aβ cascade hypothesis and the many attempted treatments thereof have failed the public. The fundamental premise of the cascade hypothesis is in question as there have been numerous failed clinical trials for disease modifying therapies targeting Aβ.[11–13]

Consequently, researchers have turned their attention to other risk factors and mechanisms that might contribute to the dementia that defines AD.[14–16] One such risk factor is apolipoprotein E (APOE) and its role in delivering cholesterol and complex lipids to neurons for membrane maintenance, neurogeneration, and repair.[17] APOE is synthesized in the brain by astrocytes, microglia, and select neurons.[18,19] The gene (APOE) that codes for APOE is polymorphic and has three common alleles (ie, ε2, ε3, and ε4) that code for three protein isoforms (ie, APOE2, APOE3, and APOE4, respectively).[20] APOE3 is the most prevalent isoform. Over the past three decades, APOE has become a major focus for AD research following the localization of APOE4 on NFT and amyloids of senile plaques in the brains of AD patients.[21] The APOE4 isoform is the greatest genetic risk factor for AD as carriers of one allele are more than twice as likely as non-carriers to develop the disease, while individuals expressing two APOE4 alleles are seven times more likely than non-carriers to develop AD.[22] Injured neurons secrete APOE to mobilize lipids for membrane repair. APOE4 is reported to increase pro-inflammatory cytokines and exacerbate neuroinflammation after injury.[23] APOE4, but not APOE3, interacts with mitochondria to reduce respiratory capacity and function compromising energy use.[24]

It has long been known that dysregulation in energy use, mitochondrial abnormalities, oxidative stress, and neuroinflammation that occur with aging are contributing factors to the pathophysiology of AD.[16] This gradual disruption in metabolism with aging is exacerbated by obesity and diabetes. Diet-induced obesity is recognized as a major factor in the etiology and pathophysiology of AD.[25–27] High-fat/high-sucrose diets often contribute to the development of insulin resistance, and dysregulation in glucose use.[28,29] Individuals with Type-2 insulin resistant diabetes have a two- to three-fold greater risk for AD.[30] The abnormal glucose metabolism leads to the increased production of reactive oxygen species (ROS), a hallmark of diabetes and AD.[31] ROS-induced lipid peroxidation can lead to neuronal damage and cell death and is thought to be a contributing factor to disease progression in AD.[32,33] These and many other studies show APOE4 together with aging and a high-fat/high-sucrose diet can create an environment of hypometabolism, mitochondrial failure, oxidative stress, and lipid peroxidation—a toxic recipe for neurodegeneration and AD.[34,35] A recent publication by Pena-Bautista et al.[36] notes the need for new biomarkers in the diagnosis of early AD and highlights the importance of lipid peroxidation.

RESEARCH IN CONTEXT

1. Systematic review: The pathophysiology contributing to Alzheimer's disease (AD) typically begins decades before any signs of cognitive dysfunction.
2. Interpretation: We observe specific changes in exhaled breath composition with the onset of the disease and we experimentally validated this change using a rat model. This rat model combined the human gene apolipoprotein E (APOE)4 with aging and Western diet.
3. Future direction: The three volatile organic compound biomarkers have shown potentials to be used for non-invasive diagnosis of AD. Future directions would be on identifying metabolism changes-related biomarkers and testing them. This type of sensors has demonstrated the sensitivity up to 1 part per quadrillion for opioid detection. Better electronics, with minimum noise, can provide faster and more accurate measurement.

In the present study we hypothesized that the combination of aging and a high-fat/high-sucrose diet in male rats with an APOE4 background would generate volatile peroxidized lipids that could be measured from exhaled gas. Electronic noses have been successfully used for diagnosis of health conditions via detection and classification of volatile organic compounds (VOCs) into one or a combination of body fluids released as a result of a disease evolvement in the human body for a variety of diseases including cancers,[37–41] AD, Parkinson's disease, inflammatory bowel disease, and diabetes. In general, exhaled breath, skin/sweat, feces, urine, saliva, breast milk, and intestinal gas are the one or a combination of the secretion pathways of VOCs emission.[42]

To test this hypothesis, we developed three gas sensors fabricated from a molecularly imprinted polymer-graphene engineered to react with alkanes and small fatty acids. Molecularly imprinted polymer can be designed to fit the geometry and chemical bonding of specific VOCs. Graphene is a two-dimensional material that can sense one electron. This sensor technology was tested on 12-month-old wild-type and human APOE4 knock-in rats on high-fat/high-sucrose diets. The exhaled breath from APOE4 rats on the high-fat/high-sucrose diet was highly sensitive to several small hydrocarbons.

2 | METHODS

2.1 | Animals

Wild-type (WT; n = 3) and human APOE ε4 knock-in (TGRA8960; n = 3) male Sprague-Dawley rats, were obtained from Horizon

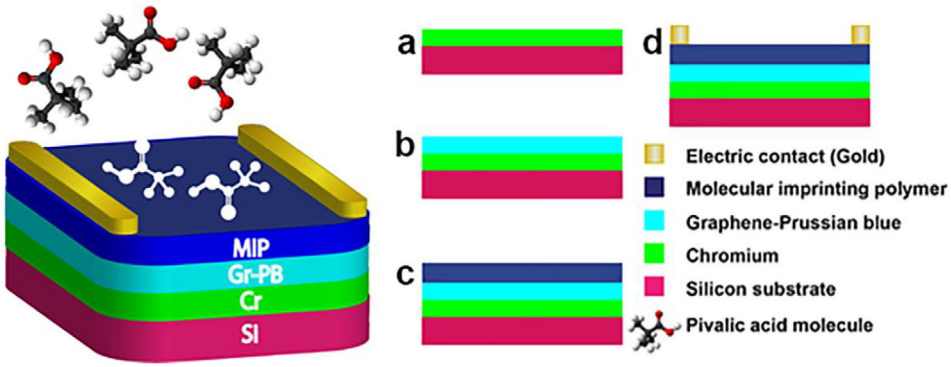

FIGURE 1 Sensor schematic. Shown is a schematic of the steps taken in the manufacture of a gas sensor. After removal of the template molecule (volatile organic compound [VOC]) from the molecular imprinting polymer (MIP) layer, there will be cavities with the exact size and shape of the template molecule (eg, pivalic acid) on the MIP surface. Steps in the fabrication process include: (A) deposition of 20 nm chromium on silicon substrate; (B) screen printing of graphene and Prussian blue layer; (C) molecular imprinting of the polymer layer formed through electro-polymerization of polypyrrole around the template biomarker molecule to be detected; and (D) 50 nm-thick gold electrode deposition and patterning

Discovery (Saint Louis, Missouri, USA). All rats were tested and imaged at 11 to 12 months of age. Rats were housed in Plexiglas cages (two per cage) and maintained in ambient temperature (22 to 24°C) on a 12:12 light:dark cycle (lights on at 07:00 am). Food and water were provided *ad libitum*. Rats were maintained on a high-fat, high-sucrose diet (HFHS) for 8 months prior to testing. The diet (TD.88137) was provided by Envigo (South Easton, Massachusetts, USA). The content by weight was 48.5% carbohydrates (34% sucrose), 21.2% fat, 17.3% protein, and 0.2% cholesterol. All rats were acquired and cared for in accordance with the guidelines published in the National Institutes of Health (NIH) Guide for the Care and Use of Laboratory Animals. All methods and procedures described below were pre-approved by the Northeastern University Institutional Animal Care and Use Committee.

2.2 | Fabrication procedure

We recently reported an electrochemical gas sensor with glassy carbon electrode as the substrate.[43] Silicon was substituted by the glassy carbon because of its compatibility with electronic devices. A 380-um thick, p-type silicon was used as the substrate. Silicon is a not conductive, so a thin layer of chromium was sputtered on the silicon substrate to improve the conductivity. The schematic of the proposed sensor is depicted in Figure 1. The details of sensor fabrications were explained step by step.[43] These breath sensors directly sense biomarker VOCs from the exhaled breath. The novel, ultra-sensitive, and highly selective sensor enables fast (seconds to minutes), low-cost, completely non-invasive, and quantitative measurement of exhaled breath. It can be connected to a smartphone through Bluetooth communication. The designed hardware measures the resistance of each sensor, converts it to concentration, and sends the results to the smartphone. Compared to other reported gas sensors, these sensors have multifold advantages: (1) The sensors have ultra-high sensitivity, which can reach a detection limit of single-digit of part per quadrillion (ppq) and are the most sensitive gas sensors ever reported. (2) The sensor is extremely selective; it only responds to the template molecules, not to other similar VOCs, water vapor, carbon dioxide, or nitrogen, which are the main components of exhaled breath. (3) It is also inexpensive and has fast response in the order of a few seconds. (4) It can be used as a hand-held system. The designed microcontroller measures the resistance of each sensor and sends it to a smartphone through the Bluetooth module. Sensitivity and selectivity of these sensors were discussed in detail elsewhere.[44,45]

2.3 | Animal testing

All the testing procedures were done while rats were confined. An apparatus was designed to restrain the rats during the experiment without obstructing their nasal passages. The design of the restraining system included a padded head support obviating the need for ear bars helping to reduce animal discomfort while minimizing motion artifact. The sensor was placed very close to the rat's mouth and the ambient air sampled over a 500-second period.

Four WT males and three APOE4 males, 11 to 12 months of age and maintained on HFHS diet were tested. Four control male rats, 4 months of age and fed normal rat chow, were also tested. The sensors were placed very closed to the rat's mouth so they could detect the chemicals exhaled by the rats.

2.4 | Neuroimaging

Imaging sessions were conducted using a Bruker Biospec 7.0T/20-cm USR horizontal magnet (Bruker, Billerica, Massachusetts, USA) and a 20-G/cm magnetic field gradient insert (ID = 12 cm) capable of a 120-μs rise time. Radio frequency signals were sent and received with a quadrature volume coil built into the animal restrainer (Animal Imaging Research, Holden, Massachusetts, USA). The design of the restraining system included a padded head support obviating the need for ear bars helping to reduce animal discomfort while minimizing

motion artifact. All rats were imaged under 1% to 2% isoflurane while keeping a respiratory rate of 40 to 50 breaths/minute. At the beginning of each imaging session, a high-resolution anatomical data set was collected using the RARE pulse sequence with the following parameters: 35 slices of 0.7 mm thickness; field of view (FOV) 3 cm; 256 × 256; repetition time (TR) 3900 milliseconds; effective echo time (TE) 48 milliseconds; NEX 3; 6 minutes 14 seconds acquisition time.

2.5 | Resting state functional connectivity

Scans were collected using a spin-echo triple-shot EPI sequence (imaging parameters: matrix size = 96 × 96 × 20 [H x W x D], TR/TE = 1000/15 milliseconds, voxel size = 0.312 × 0.312 × 1.2 mm, slice thickness = 1.2 mm, with 200 repetitions, time of acquisition 10 minutes). Preprocessing was accomplished by combining Analysis of Functional NeuroImages (AFNI_17.1.12, http://afni.nimh.nih.gov/afni/), FMRIB software library (FSL, v5.0.9, http://fsl.fmrib.ox.ac.uk/fsl/), Deformable Registration via Attribute Matching and Mutual-Saliency Weighting (DRAMMS 1.4.1, https://www.cbica.upenn.edu/sbia/software/dramms/index.html) and MATLAB (Mathworks, Natick, Massachusetts, USA). Brain tissue masks for resting-state functional images were manually drawn using 3DSlicer (https://www.slicer.org/) and applied for skull-stripping. Motion outliers (ie, data corrupted by extensive motion) were detected in the data set and the corresponding time points were recorded so that they could be regressed out in a later step. Functional data were assessed for the presence of motion spikes. Any large motion spikes were identified and removed from the time-course signals. This filtering step was followed by slice timing correction from interleaved slice acquisition order. Head motion correction (six motion parameters) was carried out using the first volume as a reference image. Normalization was completed by registering functional data to the 3D MRI Rat Brain Atlas© using affine registration through DRAMMS. The MRI rat atlas containing 173 annotated brain regions was used for segmentation. Data are reported in 166 brain areas, as seven regions in the brain atlas were excluded from analysis due to the large size of three brains. These brains fell slightly outside our imaging field of view and thus we did not get any signal from the extreme caudal tip of the cerebellum. Whole brains that contain all regions of interest (ROIs) are needed for analyses so rather than excluding the animals, we removed the brain sites across all animals. After quality assurance, band-pass filtering (0.01–0.1 Hz) was performed to reduce low-frequency drift effects and high-frequency physiological noise for each subject. The resulting images were further detrended and spatially smoothed (full width at half maximum = 0.8 mm). Finally, regressors comprised of motion outliers, the six motion parameters, the mean white matter, and cerebrospinal fluid time series were fed into general linear models for nuisance regression to remove unwanted effects.

The region-to-region functional connectivity method was performed to measure the correlations in spontaneous blood oxygenation level-dependent (BOLD) fluctuations. A network is comprised of nodes and edges; nodes being the brain ROI and edges being the connections between regions. Voxel time series data were averaged in each node based on the residual images using the nuisance regression procedure. Pearson's correlation coefficients across all pairs of nodes (14,535 pairs) were computed for each subject among all three groups to assess the interregional temporal correlations. The r-values (ranging from −1 to 1) were z-transformed using the Fisher's *Z* transform to improve normality. 166 × 166 symmetric connectivity matrices were constructed with each entry representing the strength of edge. Group-level analysis was performed to look at the functional connectivity in the experimental groups. The resulting *Z*-score matrices from one-group *t*-tests were clustered using the K-nearest neighbors clustering method to identify how nodes cluster together and form resting state networks. A *Z*-score threshold of $|Z| = 2.3$ was applied to remove spurious or weak node connections for visualization purposes.

3 | RESULTS

Figure 2 shows data on the sensitivity of the three VOC sensors (butylated hydroxytoluene [BHT], pivalic acid and 2,3-dimethylheptane). The sensitivity and specificity of the sensors were calculated based on the sensor's ability to correctly identify the APOE4 genotype. The sensitivity was calculated as 100%, specificity 100%, and accuracy of 100%. The change in resistance for each sensor is linearly correlated with the change in compound concentration with a regression coefficient near one.

Correlation matrices between 170 brain areas for rsFC between the WT HFHS diet and APOE4 HFHS are shown in Figure 3. Panel (A) shows a correlation matrix comparing the wilt-type control with the apolipoprotein E (APOE)4 genotype. The table in panel (B) shows the brain areas functionally coupled to the dorsal dentate hippocampus and their accompanying Z values. NS, not significant. The 3D images in panel (C) are a reconstruction of the brain areas from the table for each genotype. The diagonal line separates the two genotypes. The colored pixels denote specific brain areas that have significant connections to other pixels. Yellow to red indicate positive connections while blue indicates negative connections. Each pixel has its mirror image across genotypes. The brain areas with significant correlations often appear as clusters because they are contiguous in their neuroanatomy and function. The delineated, annotated areas highlight clusters that are similar or, in many cases, very different between genotypes. These primary clusters constitute major brain regions and their significant connections. For example, the delineated clusters labeled A are brain areas comprising the amygdala and hypothalamus. The connectivity within and between these areas is less in APOE4. This is also true of cluster G, the hippocampal complex. Clusters D (connections between pons and thalamus) and F (connections between thalamus and brainstem) are negative, suggesting a decoupling in functional activity when one or the other is active. Interestingly, cluster E comprising the cerebellum/brainstem reticular activating system is greater in APOE4.

The table below the matrix reports the *Z* values for both genotypes when seeding the dorsal dentate nucleus of the hippocampus. WT HFHS rats show connectivity between the hippocampal complex

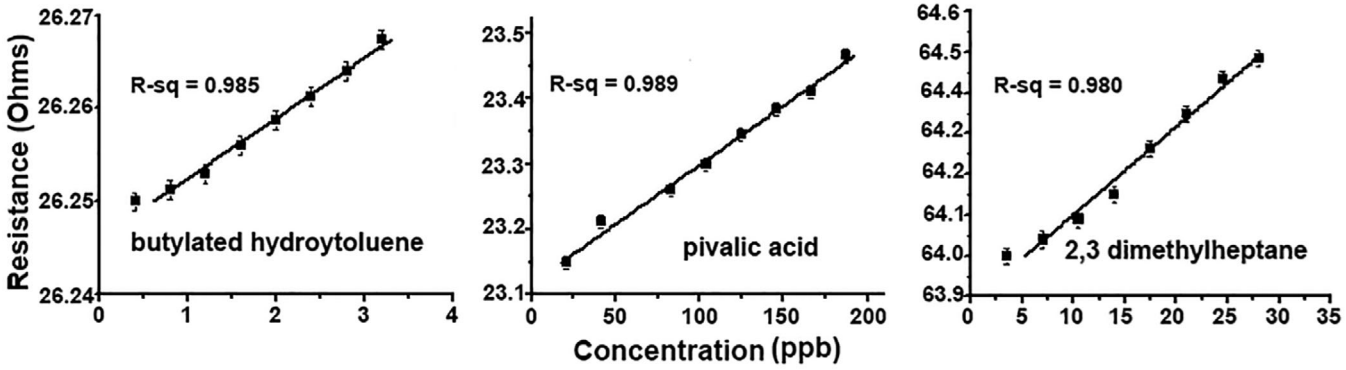

FIGURE 2 Test results on volatile organic compounds (VOCs). Results for sensing three of the published VOCs identified in exhaled breath of Alzheimer's disease patients (Tisch et al.[46]). Concentration levels are measured in parts per billion (ppb). Test molecules are butylated hydroxytoluene (BHT), pivalic acid (2,2-dimethylpropanoic acid), and 2,3-dimethylheptane. All the testing procedures were done inside a sealed chamber. The resistance was monitored while injecting specific amounts of the VOC into the chamber. Clearly, the sensitivity of the BHT sensor can go well into parts per trillion range

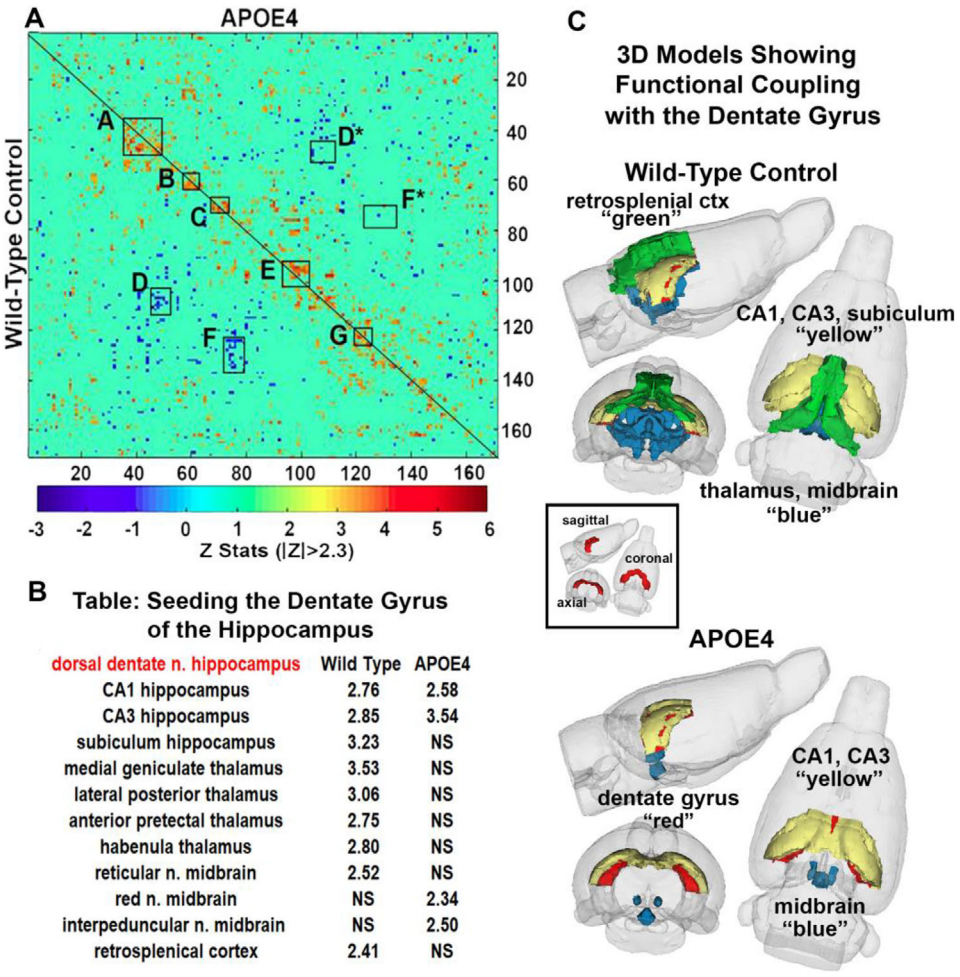

dorsal dentate n. hippocampus	Wild Type	APOE4
CA1 hippocampus	2.76	2.58
CA3 hippocampus	2.85	3.54
subiculum hippocampus	3.23	NS
medial geniculate thalamus	3.53	NS
lateral posterior thalamus	3.06	NS
anterior pretectal thalamus	2.75	NS
habenula thalamus	2.80	NS
reticular n. midbrain	2.52	NS
red n. midbrain	NS	2.34
interpeduncular n. midbrain	NS	2.50
retrosplenical cortex	2.41	NS

FIGURE 3 Functional coupling to the hippocampus. Panel (A) shows a correlation matrix comparing the wilt-type control with the apolipoprotein E (APOE)4 genotype. The table in panel (B) shows the brain areas functionally coupled to the dorsal dentate hippocampus and their accompanying *Z* values. NS, not significant. The 3D images in panel (C) are a reconstruction of the brain areas from the table for each genotype

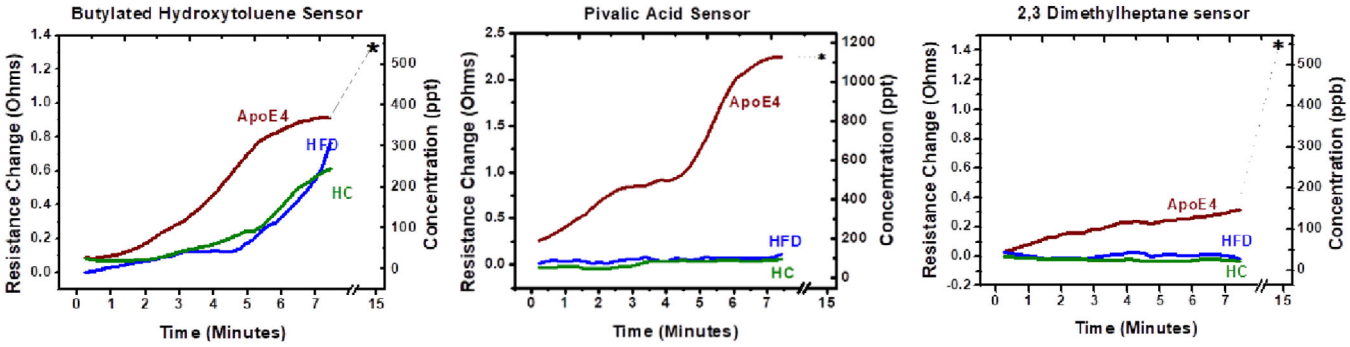

FIGURE 4 Test results from the rat model. HC is healthy control rats, HFD represents the 15-month-old rats on high fat-high sugar diet and apolipoprotein E (APOE)4 represents the 15-month-old rats with APOE4 gene on high-fat/high-sugar diet

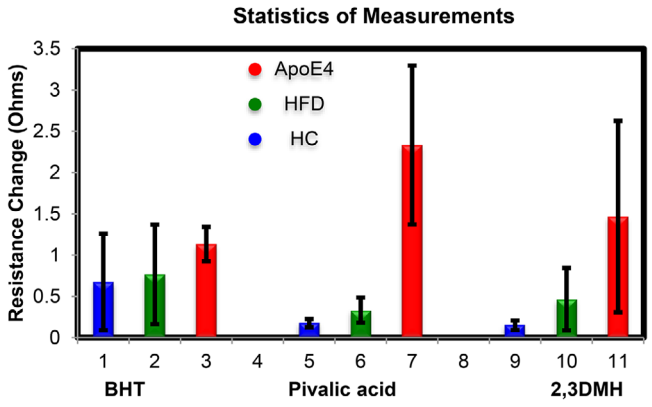

FIGURE 5 Statistical test results from the rat model. HC is healthy control rats, HFD represents the 15-month-old rats on high-fat/high-sugar diet and apolipoprotein E (APOE)4 represents the 15-month-old rats with APOE4 gene on high-fat/high-sugar diet

(CA1, CA3, subiculum) and several areas of the thalamus. APOE4 HFHS rats present with hypoconnectivity and decoupling with the thalamus. The organization of these different brain regions relative to the dorsal dentate n is shown in the 3D color coded models to the right. The small boxed insert show 3D volume of the dorsal dentate colored red in the different orthogonal views.

The results from testing the three sensors and statistal analysis of the results (BHT, pivalic acid, and 2,3-dimethyl heptane) are depicted in Figure 4 and Figure 5. Of the 11 rats tested for VOCs using the three sensors only APOE4 responded. Neither the young WT controls on a normal diet nor the old WT rats on the HFHS diet activated any of the three sensors (P-value < 1E-5) with the exception of BHT template, which did respond to all rats (Figure 4). A resistance increment of 0.3 to 2.5 ohms happened within 500 seconds of breath sampling for all sensors. By 15 minutes (dotted line and asterisk) all sensors had plateaued.

4 | DISCUSSION

Breath sensors were fabricated from a molecularly imprinted graphene polymer engineered to react with volatile alkanes and small fatty acids. Molecular imprinting is a technique to polymerize around a template molecule and remove the template after polymerization. As such it leaves cavities with the exact size and shape of the template in the polymer matrix[47] and, in this case, to fit the geometry and chemical bonding of specific VOCs. Graphene is a two-dimensional material that can sense a single electron. Graphene is highly conductive, exhibiting metallic conductivity with low Johnson noise even in the absence of charge carriers[48] so a few extra electrons can cause notable relative changes in carrier concentration. Graphene has few crystal defects,[49] which ensures a low level of excess noise. These features enable a graphene-based sensor to be capable of detecting targets in ppb level of concentration as demonstrated here.

Three key elements in molecular imprinting technique are: the target molecule (or template), which is what being sensed; the functional monomer, which is a compound having chemical and shape complementarity to the template and will help the polymerization and cross linkers. The size and shape of the cavity allow the target molecule or similar molecules to occupy the cavity, but the functional monomers orientation just allows binding with the template molecule.[50] Prussian blue (PB, ferric ferrocyanide), is an inorganic conductive material that exhibits high electrocatalytic activity and improves the electrochemical sensitivity.[51] The main mechanism of gas sensing for a graphene-based sensor is charge transfer. The sensing section acts as charge acceptor or donor that reacts to the specific gas by its resistance being changed.

Exhaled VOCs have been promoted as biomarkers to help in the diagnosis of neurodegenerative diseases. Using gas chromatography and mass spectrometry analysis, Tisch et al.[46] identified 24 unique biomarker VOCs from the breath of AD and Parkinson's patients compared to healthy controls. The same group used sensors based on functionalized nanomaterials for sensing these AD biomarker VOCs and have demonstrated 85% accuracy to distinguish AD patients from healthy controls. However, these nanomaterials-based VOC sensors are qualitative only, not selective, and rely on pattern recognition for selectivity.[43]

As proof-of-concept, three of the VOCs identified by Tisch et al. from the breath of AD patients were tested against standards in lab and in APOE4 rats as an animal model of AD. All sensors were highly sensitive and selective showing a linear change

in resistance to increasing concentrations of only their template molecule.

Interestingly, the BHT sensor was also activated by the breath of old male rats maintained on the HFHS diet while the pivalic and 2,3-dimethylheptane sensors were unresponsive to this condition. Perhaps the pivalic and 2,3-dimethylheptane sensors would have been activated by the HFHS condition had they the sensitivity of the BHT sensor. This raises an interesting question. Is the constitution of lipids and their metabolism accompanying the APOE4 genotype in rats maintained on the HFHS diet necessary and sufficient for the generation of the three VOC biomarkers identified by Tish et al. in AD patients, or could these compounds have been generated by the HFHS diet alone? Sprague-Dawley rats fed a HFHS diet for 12 months exhibit increased brain Aβ peptides and phosphorylated tau as early as 6 months of age.[29] Rats on HFHS diets develop metabolic syndrome and elements of AD.[29] The neuroinflammation and metabolic syndrome in early AD alters the chemistry of polyunsaturated fatty acids (arachidonic metabolites), conjugated fatty acids, sterols, medium-chain fatty acids, diacylglycerols, and phospholipids.[52] There is a strong relationship between lipid peroxidation and AD as plaque is strongly invested with peroxidation metabolites and fatty acids.[53,54]

Whether any of the three template compounds, BHT, pivalic acid, and 2,3-dimethylheptanae taken from the Tisch et al. study are directly linked to the dyslipidemia and lipid peroxidation associated with AD is unknown. The pivalic acid is a branched, short-chain fatty acid used in the clinic to increase the oral bioavailability of antibiotics.[55] 2,3-dimethylheptane is one of many VOCs generated by household fungus.[56] BHT can occur naturally in bacteria and some plants and is used as an additive to food and cosmetics as an antioxidant. In a recently published paper Wang et al.,[57] studying VOCs from cultures of colorectal cancer cells, reported the presence of BHT. The short-chain alkanes could possibly be by-products of lipid biochemistry but the BHT is taken as a nutritional supplement to potentially stave off dementia. Indeed, a combination of donepezil and BHT is being developed to treat AD.[58] However, it has been evidenced that this molecule can be endogenously generated by a few freshwater phytoplankton submitted to oxidative stress conditions.[59] Could the BHT detected by Tisch et al. come from dietary supplements taken by patients suffering from dementia? Perhaps, but this does not explain why our BHT sensor is sensitive to the breath of APOE4 rats on the HFHS diet. There are three possible explanations: (1) the APOE4 genotype plus HFHS does result in the production of BHT via some unknown metabolic pathway, (2) our BHT template is picking up a similar organic phenolic hydrocarbon, or (3) BHT is not a biomarker of AD. The latter possibility is most likely. The statistical parameters were calculated assuming that BHT is not a biomarker (Table 1). However, if we consider BHT as a biomarker, the sensitivity, specificity, and the accuracy will be 100%, 86%, and 88%, respectively. Although the BHT sensor was sensitive to the exhaled breath of all three rat groups, it is noticeable that the resistance change for APOE4 was the highest. So, it can be concluded that BHT is present in the rats's exhaled breath, but in higher concentration in the APOE4 cohort.

TABLE 1 Statistical parameters of VOC sensors

Statistical parameters	HFHS rat model (considering BHT is not a biomarker)	HFHS rat model (considering BHT is a biomarker)
Sensitivity	100%	100%
Specificity	100%	86%
Accuracy	100%	88%

Notes: Sensitivity = TP/(TP + FN).
Accuracy = (TP + TN)/(TP + TN + FP + FN).
TP = 33, TN = 9, FN = 0, FP = 0.
Abbreviations: BHT, butylated hydroxytoluene; FN, false negative; FP, false positive; HFHS, high-fat/high-sugar; TN, true negative; TP, true positive; VOC, volatile organic compound.

It is interesting to note that these demonstrated sensors for BHT, 2,3-dimethylheptane, and pivalic acid have sensitivities of ppt/ohm resistance change. The ultra-high sensitivity, when combined the ultra-high specificity, fast recovery in seconds in air, real-time measurement, and low cost of fabrication, these gas sensors might be able to play a very important role for early screening of dementia.

5 | SUMMARY

An array of three electrochemical gas sensors were fabricated to sense BHT, pivalic acid, and 2,3-dimethylheptane in the air at ppb level of concentration. These sensors were chosen from a group of VOCs identified from the breath of AD patients.[46] The developed electrochemical sensors exhibited excellent performance with respect to sensitivity, range of detection, selectivity, stability, and reproducibility. As proof-of-concept, the sensors were tested against the breath of APOE4 rats on a HFHS diet, an animal model of AD. All sensors were highly sensitive and selective showing a linear change in resistance to increasing concentrations of only their template molecule.

6 | LIMITATIONS AND FUTURE DIRECTIONS

As a pilot study there were two main limitations: (1) the study was underpowered and could have used a greater number of rats in each experimental group. While this would normally lead to Type II errors, that is, false negatives, the sensitivity of the sensors was such that we were able to discriminate between experimental conditions. (2) The study did not include female rats. Female carriers of APOE4 have a higher risk of developing AD than males.[60] The elimination of this sex was not by design, as only males were available for testing in this aging study.

The three VOC biomarkers have shown potential to be used for non-invasive diagnosis of AD. Future directions would be identifying metabolism changes related biomarkers and testing them. These types of sensors have demonstrated the sensitivity up to 1 ppq for opioid

detection.[61] However, the VOCs have high vapor pressure at room temperature, which limits the sensitivity of the sensor to ppb level. This type of sensor has been also demonstrated to detect explosive materials at very low concentration.[45] Better electronics, with minimum noise, can help develop faster and more accurate measurement. The goal of this research is to deliver a hand-held system that can be purchased through a pharmacy.

CONFLICTS OF INTEREST

CFF has a financial interest in Animal Imaging Research, the company that manufactures the rat imaging system. PK has a financial interest in Ekam Solutions, the company that developed the rat atlas and analytical tools.

REFERENCES

1. Wilson RS, Segawa E, Boyle PA, et al. The natural history of cognitive decline in Alzheimer's disease. *Psychol Aging*. 2012;27(4):1008-1017.
2. Matthews KA, Xu W, Gaglioti AH, et al. Racial and ethnic estimates of Alzheimer's disease and related dementias in the United States (2015-2060) in adults aged >/ = 65 years. *Alzheimers Dement*. 2019;15(1):17-24.
3. James BD, Leurgans SE, Hebert LE, Scherr PA, Yaffe K, Bennett DA. Contribution of Alzheimer disease to mortality in the United States. *Neurology*. 2014;82(12):1045-1050.
4. Hurd MD, Martorell P, Langa KM. Monetary costs of dementia in the United States. *N Engl J Med*. 2013;369(5):489-490.
5. Aisen PS, Cummings J. On the path to 2025: understanding the Alzheimer's disease continuum. *Alzheimer's Res Ther*. 2017;9(1):60.
6. Scheltens P, Blennow K, Breteler MM, et al. Alzheimer's disease. *Lancet*. 2016;388(10043):505-517.
7. Jack CR, Jr, Holtzman DM. Biomarker modeling of Alzheimer's disease. *Neuron*. 2013;80(6):1347-1358.
8. Hardy JA, Higgins GA. Alzheimer's disease: the amyloid cascade hypothesis. *Science*. 1992;256(5054):184-185.
9. Blennow K, Hampel H, Zetterberg H. Biomarkers in amyloid-beta immunotherapy trials in Alzheimer's disease. *Neuropsychopharmacology*. 2014;39(1):189-201.
10. Cummings J, Lee G, Ritter A, Zhong K. Alzheimer's disease drug development pipeline: 2018. *Alzheimers Dement (N Y)*. 2018;4:195-214.
11. Ricciarelli R, Fedele E. The amyloid cascade hypothesis in Alzheimer's disease: it's time to change our mind. *Curr Neuropharmacol*. 2017;15(6):926-935.
12. Herrup K. The case for rejecting the amyloid cascade hypothesis. *Nat Neurosci*. 2015;18(6):794-799.
13. Panza F, Lozupone M, Logroscino G, Imbimbo BP. A critical appraisal of amyloid-beta-targeting therapies for Alzheimer disease. *Nat Rev Neurol*. 2019;15(2):73-88.
14. Farber SA, Slack BE, Blusztajn JK. Acceleration of phosphatidylcholine synthesis and breakdown by inhibitors of mitochondrial function in neuronal cells: a model of the membrane defect of Alzheimer's disease. *FASEB J*. 2000;14(14):2198-2206.
15. Huang Y. Abeta-independent roles of apolipoprotein E4 in the pathogenesis of Alzheimer's disease. *Trends Mol Med*. 2010;16(6):287-294.
16. Hoyer S. Brain glucose and energy metabolism abnormalities in sporadic Alzheimer disease. Causes and consequences: an update. *Exp Gerontol*. 2000;35(9-10):1363-1372.
17. Mahley RW, Huang Y. Alzheimer disease: multiple causes, multiple effects of apolipoprotein E4, and multiple therapeutic approaches. *Ann Neurol*. 2009;65(6):623-625.
18. Mahley RW. Apolipoprotein E: cholesterol transport protein with expanding role in cell biology. *Science*. 1988;240(4852):622-630.
19. Hauser PS, Narayanaswami V, Ryan RO. Apolipoprotein E: from lipid transport to neurobiology. *Prog Lipid Res*. 2011;50(1):62-74.
20. Weisgraber KH, Rall SC, Jr, Mahley RW. Human E apoprotein heterogeneity. Cysteine-arginine interchanges in the amino acid sequence of the apo-E isoforms. *J Biol Chem*. 1981;256(17):9077-9083.
21. Namba Y, Tomonaga M, Kawasaki H, Otomo E, Ikeda K. Apolipoprotein E immunoreactivity in cerebral amyloid deposits and neurofibrillary tangles in Alzheimer's disease and kuru plaque amyloid in Creutzfeldt-Jakob disease. *Brain Res*. 1991;541(1):163-166.
22. Kuusisto J, Koivisto K, Kervinen K, et al. Association of apolipoprotein E phenotypes with late onset Alzheimer's disease: population based study. *BMJ*. 1994;309(6955):636-638.
23. Guo L, LaDu MJ, Van Eldik LJ. A dual role for apolipoprotein e in neuroinflammation: anti- and pro-inflammatory activity. *J Mol Neurosci*. 2004;23(3):205-212.
24. Liang WS, Reiman EM, Valla J, et al. Alzheimer's disease is associated with reduced expression of energy metabolism genes in posterior cingulate neurons. *Proc Natl Acad Sci U S A*. 2008;105(11):4441-4446.
25. Maesako M, Uemura K, Kubota M, et al. Environmental enrichment ameliorated high-fat diet-induced Abeta deposition and memory deficit in APP transgenic mice. *Neurobiol Aging*. 2012;33(5):1011 e1011-1023.
26. Maesako M, Uemura K, Kubota M, et al. Exercise is more effective than diet control in preventing high fat diet-induced beta-amyloid deposition and memory deficit in amyloid precursor protein transgenic mice. *J Biol Chem*. 2012;287(27):23024-23033.
27. Bhat NR, Thirumangalakudi L. Increased tau phosphorylation and impaired brain insulin/IGF signaling in mice fed a high fat/high cholesterol diet. *J Alzheimer's Dis*. 2013;36(4):781-789.
28. Baranowski BJ, Bott KN, MacPherson REK. Evaluation of neuropathological effects of a high-fat high-sucrose diet in middle-aged male C57BL6/J mice. *Physiol Rep*. 2018;6(11):e13729.
29. Niu L, Han DW, Xu RL, et al. A high-sugar high-fat diet induced metabolic syndrome shows some symptoms of Alzheimer's disease in rats. *J Nutr Health Aging*. 2016;20(5):509-513.
30. Arvanitakis Z, Wilson RS, Bienias JL, Evans DA, Bennett DA. Diabetes mellitus and risk of Alzheimer disease and decline in cognitive function. *Arch Neurol*. 2004;61(5):661-666.
31. Reddy VP, Zhu X, Perry G, Smith MA. Oxidative stress in diabetes and Alzheimer's disease. *J Alzheimer's Dis*. 2009;16(4):763-774.
32. Pratico D, Sung S. Lipid peroxidation and oxidative imbalance: early functional events in Alzheimer's disease. *J Alzheimer's Dis*. 2004;6(2):171-175.
33. Pratico D, Uryu K, Leight S, Trojanoswki JQ, Lee VM. Increased lipid peroxidation precedes amyloid plaque formation in an animal model of Alzheimer amyloidosis. *J Neurosci*. 2001;21(12):4183-4187.
34. Chen HK, Ji ZS, Dodson SE, et al. Apolipoprotein E4 domain interaction mediates detrimental effects on mitochondria and is a potential therapeutic target for Alzheimer disease. *J Biol Chem*. 2011;286(7):5215-5221.
35. Martins IJ, Hone E, Foster JK, et al. Apolipoprotein E, cholesterol metabolism, diabetes, and the convergence of risk factors for Alzheimer's disease and cardiovascular disease. *Mol Psychiatry*. 2006;11(8):721-736.
36. Pena-Bautista C, Baquero M, Vento M, Chafer-Pericas C. Free radicals in Alzheimer's disease: lipid peroxidation biomarkers. *Clin Chim Acta*. 2019;491:85-90.
37. Amal H, Leja M, Funka K, et al. Breath testing as potential colorectal cancer screening tool. *Int J Cancer*. 2016;138(1):229-236.
38. Nakhleh MK, Amal H, Jeries R, et al. Diagnosis and classification of 17 diseases from 1404 subjects via pattern analysis of exhaled molecules. *ACS Nano*. 2016;11(1):112-125.
39. Amal H, Leja M, Funka K, et al. Detection of precancerous gastric lesions and gastric cancer through exhaled breath. *Gut*. 2015;65(3):400-407. gutjnl-2014-308536.

40. Amal H, Shi DY, Ionescu R, et al. Assessment of ovarian cancer conditions from exhaled breath. *Int J Cancer*. 2015;136(6):E614-E622.
41. Nakhleh MK, Amal H, Awad H, et al. Sensor arrays based on nanoparticles for early detection of kidney injury by breath samples. *Nanomed Nanotechnol Biol Med*. 2014;10(8):1767-1776.
42. Hu W, Wan L, Jian Y, et al. Electronic noses: from advanced materials to sensors aided with data processing. *Adv Mater Technol*. 2019;4:1800488.
43. Emam S, Adedoyin A, Geng X, etal. A molecularly imprinted electrochemical gas sensor to sense butylated hydroxytoluene in air. *J Sens*. 2018;2018: 1-9.
44. Sun NX, Emam S, Ekenseair AK, Molecularly-Imprinted Electrochemical Sensors, US Patent App. 16/383,220, 2019.
45. Adams JD, Emam S, Sun N, et al. A molecularly imprinted polymer-graphene sensor antenna hybrid for ultra sensitive chemical detection. *IEEE Sens J*. 2019;19(16):6571-6577.
46. Tisch U, Schlesinger I, Ionescu R, et al. Detection of Alzheimer's and Parkinson's disease from exhaled breath using nanomaterial-based sensors. *Nanomedicine (Lond)*. 2013;8(1):43-56.
47. Lin CY, Tai DF, Wu TZ. Discrimination of peptides by using a molecularly imprinted piezoelectric biosensor. *Chemistry*. 2003;9(20):5107-5110.
48. Geim AK, Novoselov KS. The rise of graphene. *Nat Mater*. 2007;6(3):183-191.
49. Hwang EH, Adam S, Sarma SD. Transport in chemically doped graphene in the presence of adsorbed molecules. *Cond-Mat*: 0610834.
50. Li Y, Li Y, Hong M, et al. Highly sensitive protein molecularly imprinted electro-chemical sensor based on gold microdendrites electrode and prussian blue mediated amplification. *Biosens Bioelectron*. 2013;42:612-617.
51. Cui M, Liu S, Lian W, Li J, Xu W, Huang J. A molecularly-imprinted electrochemical sensor based on a graphene-Prussian blue composite-modified glassy carbon electrode for the detection of butylated hydroxyanisole in foodstuffs. *Analyst*. 2013;138(20): 5949-5955.
52. Nagao K, Yanagita T. Bioactive lipids in metabolic syndrome. *Prog Lipid Res*. 2008;47(2):127-146.
53. Benseny-Cases N, Klementieva O, Cotte M, Ferrer I, Cladera J. Microspectroscopy (muFTIR) reveals co-localization of lipid oxidation and amyloid plaques in human Alzheimer disease brains. *Anal Chem*. 2014;86(24):12047-12054.
54. Zarrouk A, Nury T, Riedinger JM, Rouaud O, Hammami M, Lizard G. Dual effect of docosahexaenoic acid (attenuation or amplification) on C22:0-, C24:0-, and C26:0-induced mitochondrial dysfunctions and oxidative stress on human neuronal SK-N-BE cells. *J Nutr Health Aging*. 2015;19(2):198-205.
55. Abrahamsson K, Holme E, Jodal U, Lindstedt S, Nordin I. Effect of short-term treatment with pivalic acid containing antibiotics on serum carnitine concentration—a risk irrespective of age. *Biochem Mol Med*. 1995;55(1):77-79.
56. Sullivan JB, Kriegr GR. *Clinical Environmental Health and Toxic Exposures*. Philadelphia: Lippincott Williams & Wilkins; 2001:1323.
57. Wang G, Li Y, Liu M, et al. Determination of volatile organic compounds in SW620 colorectal cancer cells and tumor-bearing mice. *J Pharm Biomed Anal*. 2019;167:30-37.
58. Cai P, Fang SQ, Yang HL, et al. Donepezil-butylated hydroxytoluene (BHT) hybrids as anti-Alzheimer's disease agents with cholinergic, antioxidant, and neuroprotective properties. *Eur J Med Chem*. 2018;157:161-176.
59. Bakthavachalam B, Wu JT. Production of natural butylated hydroxytoluene as anantioxidant by freshwater phytoplankton. *J Phycol*. 2008;44:1447-1454.
60. Riedel BC, Thompson PM, Diaz Brinton R. Age, apoe and sex: triad of risk of Alzheimer's disease. *J Steroid Biochem Mol Biol*. 2016;160:134-147.
61. Emam S, Nasrollahpour M, Sun N. Ultra Sensitive Detection of Oxycodone in the air. To be published.

How to cite this article: Emam S, Nasrollahpour M, Colarusso B, et al. Detection of presymptomatic Alzheimer's disease through breath biomarkers. *Alzheimer's Dement*. 2020;12:e12088. https://doi.org/10.1002/dad2.12088